How to cite: *Angew. Chem. Int. Ed.* **2021**, *60*, 17887–17892
International Edition: doi.org/10.1002/anie.202104294
German Edition: doi.org/10.1002/ange.202104294

Molecular Electronics

A Trapezoidal Octacyanoquinoid Acceptor Forms Solution and Surface Products by Antiparallel Shape Fitting with Conformational Dipole Momentum Switch

Samara Medina Rivero, Javier Urieta-Mora, Agustín Molina-Ontoria, Cristina Martín-Fuentes, José I. Urgel, Maria Zubiria-Ulacia, Vega Lloveras, David Casanova, José I. Martínez, Jaume Veciana, David Écija, Nazario Martín,* and Juan Casado**

Abstract: *A new compound (**1**) formed by two antiparallelly disposed tetracyano thienoquinoidal units has been synthesized and studied by electrochemistry, UV/Vis-NIR, IR, EPR, and transient spectroscopy. Self-assembly of **1** on a Au(111) surface has been investigated by scanning tunneling microscopy. Experiments have been rationalized by quantum chemical calculations. **1** exhibits a unique charge distribution in its anionic form, with a gradient of charge yielding a neat molecular in-plane electric dipole momentum, which transforms out-of-plane after surface deposition due to twisted→folded conformational change and to partial charge transfer from Au(111). Intermolecular van der Waals interactions and antiparallel trapezoidal shape fitting lead to the formation of an optimal dense on Au(111) two-dimensional assembly of **1**.*

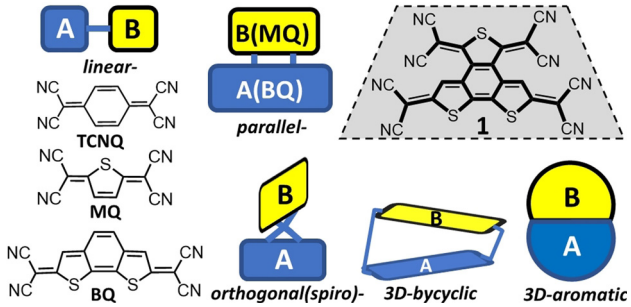

Figure 1. Coupling modes in bichromophoric systems, A and B. Tetracyano substituted thienoquinoidal **MQ** and **BQ** compounds represent the constitutional fragments of trapezoid-like compound **1** together with the benchmark tetracyano quinodimethane, **TCNQ**.

The realization of novel properties emerging upon electronic covalent coupling between chromophores (i.e., bichromophoric systems) is a critical issue for the development of photo- and electrically active systems.[1–3] In this regard, the relative topology and orientation of the π-subchromophores, such as in A + B type π-systems in Figure 1, with 1D linear conjugation, 2D parallel conjugation,[4] 3D orthogonal spiroconjugation[5] or 3D conjugation[6] are key factors. On the other hand, studies of the distribution of the excess of charge in π-conjugated moieties in post-electron transfer events are central issues in photophysics and photochemistry, in energy storage[7] and in organic electronics.[8] In addition to this electronic provision, its embedment in different molecular forms is of relevance as these can define unique ways of shape fitting in supramolecular and surface assemblies. Joint electronic and molecular shape designs thus allow to build molecular-based synthons in a tailored manner towards new bulk and nano organized materials. Accordingly, herein, we present a trapezoidal-shape molecule having a double π-electron quinoidal array, **1** in Figure 1.

[*] S. Medina Rivero, Prof. J. Casado
Department of Physical Chemistry, University of Málaga
Andalucia-Tech Campus de Teatinos s/n, 29071 Málaga (Spain)
E-mail: casado@uma.es

J. Urieta-Mora, Dr. A. Molina-Ontoria, C. Martín-Fuentes, Dr. J. I. Urgel, Prof. D. Écija, Prof. N. Martín
IMDEA-Nanociencia, C/Faraday 9
Ciudad Universitaria de Cantoblanco
28049 Madrid (Spain)
E-mail: nazmar@ucm.es

J. Urieta-Mora, Prof. N. Martín
Department of Organic Chemistry, Faculty of Chemistry
Complutense University of Madrid
28040 Madrid (Spain)

M. Zubiria-Ulacia, Dr. D. Casanova
Donostia, International Physics Center (DIPC) & IKERBASQUE—Basque Foundation for Science
Paseo Manuel de Lardizabal, 4, 20018 Donostia-San Sebastián, Euskadi (Spain)

Dr. V. Lloveras, Prof. J. Veciana
Department of Molecular Nanoscience and Organic Materials, Institut de Ciència de Materials de Barcelona (ICMAB-CSIC) and Networking Research Center on Bioengineering, Biomaterials and Nanomedicine (CIBER-BBN)
Campus de la UAB, 08193 Bellaterra (Spain)
E-mail: vecianaj@icmab.es

Dr. J. I. Martínez
Department of Nanostructures and Low-dimensional Materials, Institute of Materials Science of Madrid (ICMM-CSIC)
Ciudad Universitaria de Cantoblanco
C/Sor Juana Inés de la Cruz 3, 28049 Madrid (Spain)

Supporting information and the ORCID identification number(s) for the author(s) of this article can be found under: https://doi.org/10.1002/anie.202104294.

Recently, the inspection of the organization of organic π-conjugated molecules on surfaces is a major topic of research given the emerging features of the adsorbates, their assemblies and surface reactivity.[9–15] In spite of the relevance of on-surface discoveries, connections between solution properties of molecules and their behaviors on surfaces become mandatory to develop a rational and unified understanding of both worlds. We show here how the trapezoidal shape of **1** provides basic driving forces for the assembly mode on surface. The vanguard double antiparallel quinoid concept of **1** stresses on the efforts towards fine control of intramolecular properties, but also on the necessity of acting on new molecular forms pursuing intermolecular shape fitting which could bring on the table emerging ways to control assembly properties. For instance, our study of **1** discloses the ability to tailor the electrical dipole momentum of the species from solution to the surface driven by changes in the molecular conformation.

Solution studies on **1** have been carried out by stationary infrared and time-resolved transient infrared (TRIR technique)[16] spectroscopies. The presence of cyano groups in **1**, through their C≡N stretching frequency [ν(C≡N)], has provided the way for electron distribution studies.[17–22] On the other hand, on-surface studies of **1** have been carried out on a relatively weak interacting Au(111) surface by scanning tunneling microscopy (STM) under ultra-high vacuum (UHV) conditions, which have led to the formation of an optimal dense on-surface 2D antiparallel molecular assembly.

The new 2D π-conjugated **1** is formed by coupling of two thienoquinoidal cores in antiparallel fashion: a tetracyano quinoidal thiophene[23] (**MQ**) and a tetracyano quinoidal bithiophene[24] (**BQ**) in Figure 1, the three thiophenes surrounding a benzenoid ring (i.e., generating a trapezoidal-like form).[25,26] Tetracyanoquinoidal or tetracyanoquinodimethane (TCNQ)-based π-extended molecules are important electroactive units in the field of organic conductors[18–24] and organic electronics.[27] With **1** we wish to address the following issues: 1) the shape of the electron distribution in its anionic species by spectroelectrochemistry; and 2) the way in which the trapezoidal shape of **1** dictates its 2D organization on a relatively weak interacting surface; 3) the influence of conformation in the direction of the electrical dipole momentum upon adsorption. The aforementioned experimental information will be underpinned by quantum chemical modeling.

The synthetic route to compound **1** starts with the tetrabrominated *bbc*-benzotrithiophene derivative which was synthesized according to previously reported protocols (see ESI for details). With this central scaffold in hand, **1** was readily prepared by reaction with tetracyanoethylene oxide and copper in refluxing 1,2-dibromoethane in 18% yield (characterization in the Supporting Information, Figures S1–S3).

The electronic absorption spectrum of **1** is shown in Figure 2. It displays two main absorptions at 425 and 538 nm, in fairly good agreement with the absorption profiles simulated at different computational levels (Table S1 and Figure S4). **1** presents two structural conformers. The most stable form has an optimized geometry featuring a dihedral

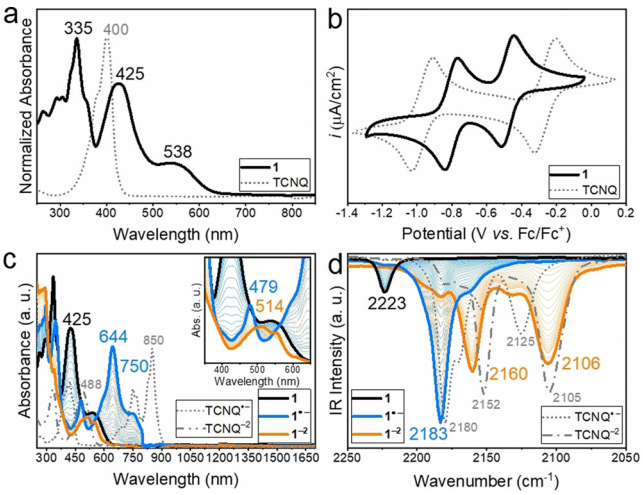

Figure 2. a) UV/Vis absorption spectrum of **1** and TCNQ, and b) their cyclic voltamograms in CH_2Cl_2 0.1 M PF_6NBu_4. Spectroelectrochemical measurements of **1** and TCNQ in the cathodic wave carried out in CH_2Cl_2 0.1 M PF_6NBu_4. c) UV/Vis-NIR spectra and d) infrared spectra.

angle of about 20° (twisted conformer in Figure 3, and Figure S5) between the planes containing the two subchromophores owing to the steric crowding between the dicyano groups of the two quinoidal moieties. The second local minimum exhibits a folded structure with CN groups of the two moieties (**MQ** and **BQ**) pointing towards the same side regarding the main molecular plane, which is computed at $\Delta G° = 1.4$ kcal mol^{-1} above the twisted conformer. The interconversion between the two forms can be achieved by surmounting an energy barrier of $\Delta G^{\neq} = 5.0$ kcal mol^{-1} with respect to the twisted minimum. In general, computed electronic structure properties for the two conformers are rather similar. Comparison between the two forms can be found in the Supporting Information (Figures S6–S8, and Tables S2–S4). Another aspect of **1** is that its closed-shell wavefunction is slightly unstable by 1.23 kcal mol^{-1} with respect to the open-shell broken symmetry solution at the UB3LYP/6-31G** level of calculation disclosing a ground state open-shell singlet with the lowest triplet at 5.33 kcal mol^{-1} (4.50 kcal mol^{-1} at UB3LYP/6–31 + G(d) level in vacuum and 6.52 kcal mol^{-1} in solution).

The cyclic voltammogram of **1** is in Figure 2 which, such as TCNQ, shows two consecutive reversible one-electron processes. Interestingly, TCNQ shows its first potential reduction earlier than **1**, while **1** displays its second reduction before TCNQ. Regarding the first reduction, the aromaticity recov-

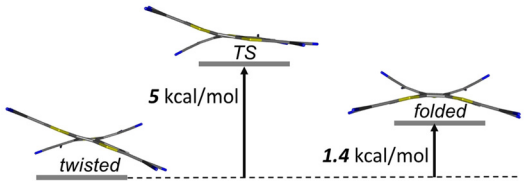

Figure 3. Relative Gibbs free energies of the twisted and folded conformers, and the transition state (TS) for their interconversion for the ground state of the neutral species of **1**.

ery of benzene in TCNQ might be greater than the sum of the aromaticity recoveries in the **BQ**/**MQ** moieties due to the competition effect. The situation is reversed in the second reduction owing to the larger mitigation of electrostatic repulsion in the dianion of **1** than in that of TCNQ. Further reduction of $\mathbf{1}^{-2}$ (Figure S9) is observed at more cathodic potentials.

UV/Vis-NIR absorption spectroelectrochemistry of **1** in Figure 2 (spectroelectrochemical UV/Vis-NIR details in Figure S12 and theoretical bands assignment in Tables S6 and S7) shows that initial reduction produces the disappearance of the neutral bands and the development of a spectrum characterized by three new ones at 479, 644, and 750 nm. Further charging gives way to the growth of only one new band at 514 nm. Infrared spectroelectrochemistry of **1** in the region of the ν(C≡N) band is also shown in Figure 2. The IR band of neutral **1** at 2223 cm^{-1} gives rise to a very strong and broad band at 2183 cm^{-1} in $\mathbf{1}^{\bullet-}$, a spectrum which is similar (i.e., 2180 cm^{-1}) to that of the radical anion of TCNQ[28] also displayed in Figure 2 (spectroelectrochemical IR reductions of **1** in Figure S13 with theoretical IR calculations in Figures S14 and S15, and spectroelectrochemical UV/Vis-NIR and IR for TCNQ in Figures S16 and S17) confirming that most of the anionic charge in $\mathbf{1}^{\bullet-}$ is distributed between the dicyanomethylene groups of the **BQ** moiety (with a smaller amount on **MQ**). Interestingly, this charge distribution generates a permanent electric dipole moment in $\mathbf{1}^{\bullet-}$ such as revealed in Figure S11 from calculations. Posterior electrochemical reduction of $\mathbf{1}^{\bullet-}$ produces a spectrum with two well defined IR absorptions at 2160 and 2106 cm^{-1} which compare with the 2152/2105 cm^{-1} pair in the dianion of TCNQ confirming that a larger portion of the negative charge in $\mathbf{1}^{-2}$ is on the cyano groups of the **BQ** moiety (see Table S5 and Figure S10 for charge distribution analysis). To further rationalize this, we carried out quantum chemical calculations on the structures of Figure 4. **D1**, **D1a** and **D1b**. DFT calculations predict the most stable form to be **D1** followed by **D1a**, and **D1b** (Table S8). In addition, such calculations show that the ground state of $\mathbf{1}^{-2}$ is a closed-shell singlet with a rather large energy gap to the triplet (Table S9). The reduction of the electronic repulsion of the negative charges by spreading them around the whole structure of **1** together with the recovery of the aromaticity in the central benzene and in two thiophenes in **D1** might justify its larger stabilization (Tables S10 and S11 for the bond length and NICS changes on reduction). The final situation is that either in $\mathbf{1}^{\bullet-}$ or $\mathbf{1}^{-2}$ there is a larger amount of charge on the **BQ** moiety than in **MQ** or negative charge gradient (see Figure 4) that will produce an in-plane electric dipole moment in the charged species.

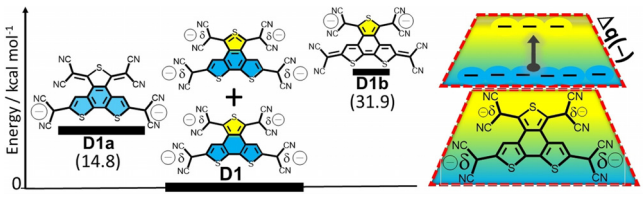

Figure 4. Left: Relative energies of the dianion species of **1** showing the qualitative charge distribution on its optimized geometry, **D1**, and **D1a** and **D1b**, which are the forms with the charge constrained in the **BQ** and **MQ** units, respectively. Right: drawn of the negative charge gradient (qualitatively marked by the blue-yellow colors change) in the dianion of **1** according to calculations in Table S5 and Figure S10. The arrow marks the electric dipole momentum generated (Figure S11).

The reduction process was followed by electron paramagnetic resonance (EPR) spectroscopy (Figure 5). The neutral species of **1** was EPR silent in solution at room temperature in accordance with its singlet ground state. However, upon first reduction, the generated species possesses a neat EPR spectrum at $g = 2.0020$ composed of 9 main

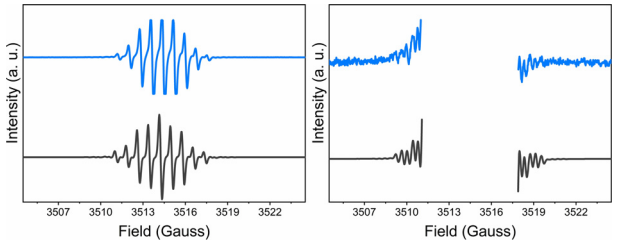

Figure 5. Left: EPR experimental (blue) spectrum of the first reduced species of **1** and simulated (gray) spectrum of the radical anion of **1**. Right: enlarged experimental and simulated spectra where satellite lines, due to the coupling with the ^{33}S nuclei, are shown.

lines due to the coupling of the unpaired electron with N and H nuclei of the **BQ** moiety. This species also shows weak emerging satellite lines as a result of the coupling of the unpaired electron with the ^{33}S nuclei (isotope abundance 0.75 %) of **BQ** and **MQ** moieties (Table S12). These results evidence that the charge is mostly delocalized on the **BQ** moiety with a residual amount on **MQ**, such as discussed above. The dianion does not give EPR signal due to the singlet ground state.

The transient electronic absorption spectra (or excited state absorptions, ESA bands) of **1** in the pico-second time regime are shown in Figure S18 (Table S13 for excited state calculations). The observed rise and decay times correspond to ultrafast excited state processes justifying the absence of fluorescence of **1**. Interestingly, the time resolved spectra show the simultaneous rise of two ESA bands at 520 nm and at 660 nm. The femtosecond excited state absorption spectrum of TCNQ[29] in acetonitrile features a main absorption at 460 nm with a major decay time of hundreds of femtoseconds followed by a secondary long component of 24 ps. The TRIR spectra of **1** in the interval of tens of picoseconds show a strong infrared absorption that initially displays its maximum at ≈2170 cm^{-1} and that progresses with time with a displacement up to 2181 cm^{-1}. The appearance of the infrared band at values close to that of the radical anion could be ascribed to a symmetry breaking effect in the excited state due to equalization of the CC bonds in the conjugated path followed by pseudo Jahn Teller distortion along a suitable backbone CC stretchimg vibration. The distortion of such fused rigid core is feasible by out-of-plane distortions of the outermost CN groups that localize the excitation distortion (producing large changes of the ν(C≡N) wavenumbers) and

minimizes steric crowding. This structure might resemble that of the folded structure of **1** in Figure 4 revealing a fluxional twisted→folded conversion upon photexcitation.

We have further characterized **1** upon adsorption on a relatively weak interacting surface such as Au(111). For this purpose, a submonolayer coverage of **1** is deposited onto an atomically clean Au(111) surface held at room temperature under ultra high vacuum conditions. The STM image displayed in Figure 6a shows molecules self-assembled into close-packed islands. This antiparallel top&down organization is primarily promoted by the trapezoidal shape of **1** and it is intermolecularly fastened by van der Waals interactions between adjacent species. Such self-assembly is in agreement with DFT simulations of a supramolecular domain (see the Supporting Information).

To study an isolated molecule, we have performed STM manipulation experiments, by laterally displacing the STM tip at close tip-sample distances across the edge of a molecular island (Figure S19). A high resolution image is shown in Figure 6b, revealing a T trapezoidal molecular shape together with two bright peripheral lobes with a maximum apparent height of 2.2 Å (measured at a sample bias of −0.5 V). The experimental features, observed in Figure 6b, are well reproduced by the DFT optimized geometry and the corresponding Keldish–Green STM simulation of **1** on the Au(111) surface (Figures 6c,d). According to optimized model in Figure 6d, a single molecule of **1** adopts on-surface a highly nonplanar configuration corresponding to the metastable folded conformer obtained in vacuum (Figure 3). In the **BQ** moiety, one CN of each dicyano group is bent towards the surface, establishing CN···Au interactions, while the other vicinal CN is displaced upright. In the **MQ** moiety the CN groups are both bent pointing to the same side. Furthermore, the S atom of the **MQ** unit is closer to the surface, likely by S···Au interaction. Altogether, the molecules adopt a nonplanar folded conformation which provokes the appearance of a waving-like tiled roof aspect for the surface assembly.

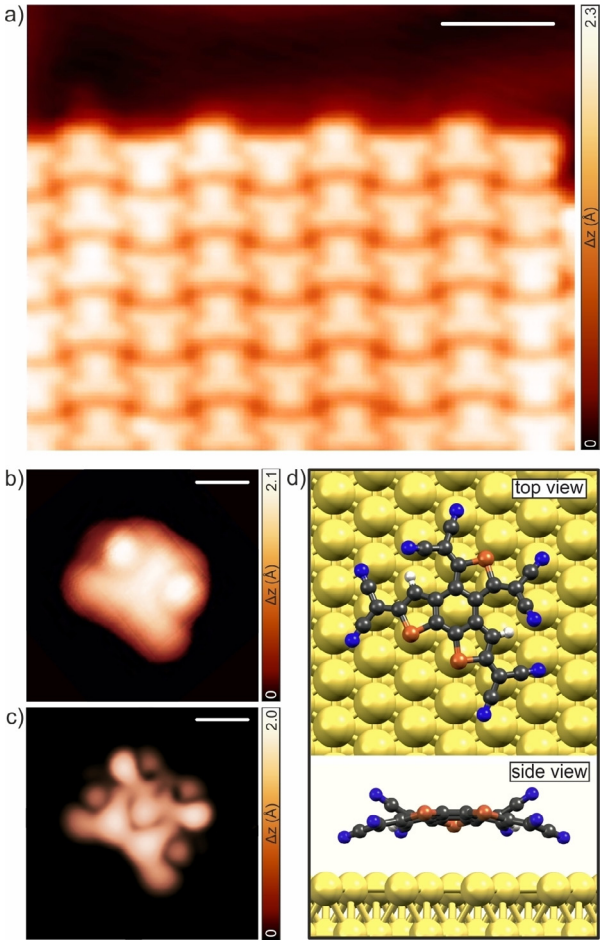

Figure 6. Structural characterization of **1** on Au(111). a) Self-assembled island of **1** after sublimation on the gold surface held at room temperature. $V_b = -0.5$ V, $I_t = 80$ pA, scale bar = 3 nm. b) Magnified view of an isolated molecular species evidencing its T-shape appearance with two bright peripheral lobes. $V_b = -0.5$ V, $I_t = 100$ pA, scale bar = 0.5 nm. c) Simulated Keldish-Green STM image of the molecule/Au(111) interface. d) Top (upper panel) and side (lower panel) views of the DFT-optimized geometry of **1** on Au(111).

Furthermore, our DFT simulations of an individual molecule and supramolecular assembly of **1** on Au(111) reveal the following conclusions: 1) adsorption energies per molecule of 1.62 eV in the simulated layer and of 1.9 eV in the single molecule; 2) an intermolecular interaction per molecule of 0.32 eV stabilizing the waving-like self-assembled arrangement (Figure S20); 3) **1** as a single molecule is predicted with a folded structure with an adsorption height of 3.0 Å largely stabilized with respect to the twist form due to the steric hindrance between the two hydrogens and the two CN groups.

In addition, we performed a Bader's charge analysis[30] based on the DFT charge density distribution, obtaining a charge transfer of 0.40 e^- from the metal surface to a single molecule of **1** which is slightly reduced to 0.37 e− in the self-assembled layer both confirming the acceptor character of **1** even on the metal surface. Interestingly, it is worth remarking that the electronic molecular in-plane dipole momentum of the planar conformer of **1** in solution dramatically changes upon adsorption on Au(111), adopting an out-of-plane disposition pointing perpendicularly down from the molecule towards the surface with a net computed value of 0.45 D for the single molecule and of 0.53 D in the simulated ad-layer. This in→out switch of the dipolar momentum has its origin in the confluence of two major factors: 1) the on-surface induced molecular distortion that produces a charge redistribution within the molecule unbalanced between both molecular basal planes, and 2) the charge transferred from the substrate, computed in 0.40 and 0.37 e^- for individual and self-assembled species, respectively. Part of this transferred charge redistributes within the molecule and another part accumulates on the linking molecule-substrate domains. In an intuitive scenario, one could visualize the gas phase twisted molecules approaching to the substrate during deposition and adopting the structure of the folded conformer upon adsorption, switching the electric dipole momentum orientation in the process. This phenomenon opens the door to additional tunning capabilities in designing molecular assemblies by switching the dipole momentum orientation upon surface adsorption with the subsequent modulation/impact in the electric, optical and chemical properties.

In summary, we have prepared a new acceptor molecule formed by two antiparallelly embedded tetracyano thienoquinoidal moieties. In the negative charged species, the two subchromophores compete in the stabilization of negative charge giving rise to an asymmetric distribution of charge that generates a **BQ**(more negative)→**MQ**(less negative) intramolecular in-plane charge gradient. Additionally, the self-assembly of **1** has been studied on Au(111), where, such as in solution, the molecular species retains a nonplanar conformation also featuring a Au(111)→**1** charge transfer of 0.4 electrons. Interestingly, molecular in-plane dipole momentum in solution switches to an out-of-plane orientation on the surface. The adequate molecular shape fitting, together with the emerging intermolecular interactions promote the compact top&down disposition of the trapezoidal structure of **1** among contiguous molecules in a tiled roof surface covering. This kind of studies serves to understand the physical and chemical properties that guide the molecular behavior in solution and in surfaces thus contributing to jointly rationalize both worlds, while opening new avenues for tuning properties such as the electrical dipole momenta.

Acknowledgements

The authors thank the Spanish Ministry of Science, Innovation and Universities MCIU (projects CTQ2017-83531-R, RED2018-102815-T, MAT2017-85089-C2-1-R), Centro de Excelencia Severo Ochoa grants (SEV-2016-0686, SEV-2015-0496 and FUNFUTURE CEX2019-000917-S) and the CAM (QUIMTRONIC-CM project Y2018/NMT-4783). We thank MINECO/FEDER of the Spanish Government (projects PGC2018-098533-B-100 and PID2019-109555GB-I00), the Eusko Jaurlaritza (Basque Government, project PIBA19-0004) and the Junta de Andalucía, Spain (UMA18FEDERJA057). We also thank the Research Central Services (SCAI) of the University of Málaga and the Donostia International Physics Center (DIPC) Computer Center. We thank Dr. Juwon Oh and Prof. Donhgo Kim from the Spectroscopy Laboratory for Functional π-electronic Systems and Department of Chemistry, Yonsei University in Korea for the generous gift of the TRIR and UV/Vis transient absorption spectroscopy data.

Conflict of Interest

The authors declare no conflict of interest.

Keywords: charged anions · parallel conjugation · surface STM analysis · tetracyano quinoidal compounds · vibrational and electronic spectroscopy

[1] G. Scholes, P. Ghiggino, *J. Photochem. Photobiol. A* **1994**, *80*, 355 – 362; see the special issue on Functional Molecules for electronics/optoelectronics in *Adv. Mater.* **2012**, *24*, issue number 5.

[2] a) B. J. Walker, A. J. Musser, D. Beljonne, R. H. Friend, *Nat. Chem.* **2013**, *5*, 1019 – 1024; b) J. Zirzlmeier, D. Lehnherr, P. B. Coto, E. T. Chernick, R. Casillas, B. S. Basel, M. Thoss, R. R. Tykwinski, D. M. Guldi, *Proc. Natl. Acad. Sci. USA* **2015**, *112*, 5325 – 5330; c) S. N. Sanders, E. Kumarasamy, A. B. Pun, M. T. Trinh, B. Choi, J. Xia, E. J. Taffet, J. Z. Low, J. R. Miller, X. Roy, X. Y. Zhu, M. L. Steigerwald, M. Y. Sfeir, L. M. Campos, *J. Am. Chem. Soc.* **2015**, *137*, 8965 – 8972.

[3] C. Qin, K. Goushi, F. Bencheikh, T. Komino, M. Leyden, A. S. D. Sandanayaka, C. Adachi, *Adv. Mater.* **2018**, *30*, 1802662.

[4] M. L. Kirk, D. A. Shultz, D. E. Stasiw, D. Habel-Rodriguez, B. Stein, P. D. Boyle, *J. Am. Chem. Soc.* **2013**, *135*, 14713 – 14725.

[5] a) H. E. Simmons, T. Fukunaga, *J. Am. Chem. Soc.* **1967**, *89*, 5208 – 5215; b) R. Hoffmann, A. Imamura, G. D. Zeiss, *J. Am. Chem. Soc.* **1967**, *89*, 5215 – 5220; c) P. Sandín, A. Martínez-Grau, L. Sánchez, C. Seoane, R. Pou-Amérigo, E. Ortí, N. Martín, *Org. Lett.* **2005**, *7*, 295 – 298.

[6] a) M. Bühl, A. Hirsch, *Chem. Rev.* **2001**, *101*, 1153 – 1183; b) Y. Ni, T. Y. Gopalakrishna, H. Phan, T. Kim, T. S. Herng, Y. Han, T. Tao, J. Ding, D. Kim, J. Wu, *Nat. Chem.* **2020**, *12*, 242 – 248.

[7] Y. Morita, S. Suzuki, K. Sato, T. Takui, *Nat. Chem.* **2011**, *3*, 197 – 204.

[8] a) A. Molina-Ontoria, M. Wielopolski, J. Gebhardt, A. Gouloumis, T. Clark, D. M. Guldi, N. Martín, *J. Am. Chem. Soc.* **2011**, *133*, 2370 – 2373; b) M. Wielopolski, A. Molina-Ontoria, C. Schubert, J. T. Margraf, E. Krokos, J. Kirschner, A. Gouloumis, T. Clark, D. M. Guldi, N. Martín, *J. Am. Chem. Soc.* **2013**, *135*, 10372 – 10381; c) A. Ferrer-Ruiz, T. Scharl, P. Haines, L. Rodríguez-Pérez, A. Cadranel, M. Á. Herranz, D. M. Guldi, N. Martín, *Angew. Chem. Int. Ed.* **2018**, *57*, 1001 – 1005; *Angew. Chem.* **2018**, *130*, 1013 – 1017; d) M. Izquierdo, B. Platzer, A. J. Stasyuk, O. A. Stasyuk, A. A. Voityuk, S. Cuesta, M. Solà, D. M. Guldi, N. Martín, *Angew. Chem. Int. Ed.* **2019**, *58*, 6932 – 6937; *Angew. Chem.* **2019**, *131*, 7006 – 7011.

[9] J. Barth, G. Costantini, K. Kern, *Nature* **2005**, *437*, 671 – 679.

[10] R. Otero, J. M. Gallego, A. L. V. de Parga, N. Martín, R. Miranda, *Adv. Mater.* **2011**, *23*, 5148 – 5176.

[11] L. Dong, Z. Gao, N. Lin, *Prog. Surf. Sci.* **2016**, *91*, 101 – 135.

[12] D. Écija, J. I. Urgel, A. P. Seitsonen, W. Auwärter, J. V. Barth, *Acc. Chem. Res.* **2018**, *51*, 365 – 375.

[13] W. Auwärter, D. Écija, F. Klappenberger, J. V. Barth, *Nat. Chem.* **2015**, *7*, 105 – 120.

[14] Q. Shen, H.-Y. Gao, H. Fuchs, *Nano Today* **2017**, *13*, 77 – 96.

[15] D. P. Goronzy, M. Ebrahimi, F. Rosei, Arramel, Y. Fang, S. De Feyter, S. L. Tait, C. Wang, P. H. Beton, A. T. S. Wee, P. S. Weiss, D. F. Perepichka, *ACS Nano* **2018**, *12*, 7445 – 7481.

[16] a) J. Oh, Y. Mo Sung, H. Mori, S. Park, K. Jorner, H. Ottossom, J. M. Lim, A. Osuka, D. Kim, *Chem* **2017**, *3*, 870 – 880; b) Y. M. Sung, M. C. Yoon, J. M. Lim, H. Rath, K. Noada, A. Osuka, D. Kim, *Nat. Chem.* **2015**, *7*, 418 – 422.

[17] a) J. S. Chappell, A. N. Bloch, W. A. Bryden, M. Maxfield, T. O. Poehler, D. O. Cowan, *J. Am. Chem. Soc.* **1981**, *103*, 2442 – 2443; b) M. S. Khatkale, J. P. Devlin, *J. Chem. Phys.* **1979**, *70*, 1851 – 1859.

[18] T. M. Pappenfus, J. D. Raff, E. J. Hukkanen, J. R. Burney, J. Casado, S. M. Drew, L. L. Miller, K. R. Mann, *J. Org. Chem.* **2002**, *67*, 6015 – 6024; J. Casado, L. L. Miller, K. R. Mann, T. M. Pappenfus, H. Higuchi, E. Orti, B. Milian, R. Pou-Amerigo, V. Hernandez, J. T. L. Navarrete, *J. Am. Chem. Soc.* **2002**, *124*, 12380 – 12388.

[19] a) R. Ponce Ortiz, J. Casado, V. Hernández, J. T. L. Navarrete, P. M. Viruela, E. Ortí, K. Takimiya, T. Otsubo, *Angew. Chem. Int. Ed.* **2007**, *46*, 9057 – 9061; *Angew. Chem.* **2007**, *119*, 9215 – 9219; b) P. M. Burrezo, J. L. Zafra, J. T. L. Navarrete, J. Casado, *Angew. Chem. Int. Ed.* **2017**, *56*, 2250 – 2259; *Angew. Chem.* **2017**, *129*, 2286 – 2296.

[20] J. Kim, J. Oh, S. Park, J. L. Zafra, J. R. DeFrancisco, D. Casanova, M. Lim, J. D. Tovar, J. Casado, D. Kim, *Nat. Commun.* **2019**, *10*, 4983.

[21] T. Takahashi, K. Matsuoka, K. Takimiya, T. Otsubo, Y. Aso, *J. Am. Chem. Soc.* **2005**, *127*, 8928 – 8929.
[22] a) C. Zhang, S. Medina Rivero, W. Liu, D. Casanova, X. Zhu, J. Casado, *Angew. Chem. Int. Ed.* **2019**, *58*, 11291 – 11295; *Angew. Chem.* **2019**, *131*, 11413 – 11417; b) D. Yuan, D. Huang, S. Medina Rivero, A. Carreras, C. Zhang, Y. Zou, X. Jiao, C. R. McNeill, X. Zhu, C. Di, D. Zhu, D. Casanova, J. Casado, *Chem* **2019**, *5*, 964 – 976.
[23] a) M. L. Kaplan, R. C. Haddon, F. B. Bramwell, F. Wudl, J. H. Marshall, D. O. Cowan, S. Gronowitz, *J. Phys. Chem.* **1980**, *84*, 427 – 435; b) K. Yui, Y. Aso, T. Otsubo, F. Ogura, *Bull. Chem. Soc. Jpn.* **1989**, *62*, 1539 – 1546.
[24] S. Yoshida, M. Fujii, Y. Aso, T. Otsubo, F. Ogura, *J. Org. Chem.* **1994**, *59*, 3077 – 3081.
[25] a) A. Konishi, Y. Hirao, M. Nakano, A. Shimizu, E. Botek, B. Champagne, D. Shiomi, K. Sato, T. Takui, K. Matsumoto, H. Kurata, T. Kubo, *J. Am. Chem. Soc.* **2010**, *132*, 11021 – 11023; b) A. Konishi, Y. Hirao, K. Matsumoto, H. Kurata, R. Kishi, Y. Shigeta, M. Nakano, K. Tokunaga, K. Kamada, T. Kubo, *J. Am. Chem. Soc.* **2013**, *135*, 1430 – 1437; c) W. Zeng, H. Phan, T. S. Herng, T. Y. Gopalakrishna, N. Aratani, Z. Zeng, H. Yamada, J. Ding, J. Wu, *Chem* **2017**, *2*, 81 – 92.
[26] S. N. Intorp, M. Hodecker, M. Müller, O. Tverskoy, M. Rosenkranz, E. Dmitrieva, A. A. Popov, F. Rominger, J. Freudenberg, A. Dreuw, U. H. F. Bunz, *Angew. Chem. Int. Ed.* **2020**, *59*, 12395 – 12400; *Angew. Chem.* **2020**, *132*, 12505 – 12510.
[27] a) T. M. Pappenfus, R. J. Chesterfield, C. D. Frisbie, K. R. Mann, J. Casado, J. D. Raff, L. L. Miller, *J. Am. Chem. Soc.* **2002**, *124*, 4184 – 4185; b) J. C. Ribierre, S. Watanabe, M. Matsumoto, T. Muto, A. Nakao, T. Aoyama, *Adv. Mater.* **2010**, *22*, 4044 – 4048.
[28] This ν(C≡N) band is reproduced by the computed IR active modes as two nearly degenerate antisymmetric CN stretching modes, respectively localized on **MQ** and **BQ** moieties.
[29] L. Ma, P. Hu, C. Kloc, H. Sun, M. E. Michel-Beyerle, G. G. Gurzadyan, *Chem. Phys. Lett.* **2014**, *609*, 11 – 14.
[30] R. Bader in Atoms in Molecules: A Quantum Theory, Oxford University Press, Oxford, 1994.

Manuscript received: March 27, 2021
Accepted manuscript online: June 4, 2021
Version of record online: July 7, 2021

